ANALYSIS OF THE MIGDAL TRANSFORMATION FOR MODELS WITH HEISENBERG SPINS ON A d-DIMENSIONAL LATTICE

B. SCHOENMAKER and Th.W. RUIJGROK

Institute for Theoretical Physics, Rijksuniversiteit at Utrecht, Princetonplein 5,
P.O. Box 80.006, 3508 TA Utrecht, The Netherlands

We show for classical Heisenberg spins, with a general nearest neighbour interaction, that in the Migdal approximation the only low-temperature phase transitions are Ising ones (ferro- or antiferromagnetic). For $d = 2$ neither the pure Heisenberg model nor the Lebwohl–Lasher model show a phase transition at a finite temperature. For $d > 2$ transitions do exist at intermediate temperature and the complete flow diagram together with a two-parameter phase diagram is obtained numerically for $d = 3$. Apart from critical temperatures and thermal exponents, also the magnetic exponents (for both Heisenberg and XY spins) are calculated. The latter are in very good agreement with exact results.

1. Introduction

In this paper we use the Midgal renormalisation scheme [1] to study classical three-dimensional spins (Heisenberg spins) with general interaction on a d-dimensional hypercubic lattice. The case of planar spins was treated in two previous papers [2, 3]. In that case many low-temperature phase transitions were found, which turned out to be $Z(N)$ transitions for discrete spins, and complicated flow diagrams were obtained. It seemed therefore of interest to extend the results of a preliminary study [4] of the Heisenberg case and perform a more detailed investigation of all possible phase transitions.

We consider the most general interaction, which only depends on the angle between two neighbouring spin vectors:

$$-\beta H = \sum_{(i,j)_{\text{n.n.}}} h(S_i \cdot S_j) \,. \tag{1.1}$$

The Migdal transformation for the d-dimensional lattice with scale factor $\lambda = 2$ is given by

$$\exp[h_{n+1}(S_1 \cdot S_2)] = \exp(-g_n) \int dS_3 \exp[2^{d-1}(h_n(S_1 \cdot S_3) + h_n(S_3 \cdot S_2))] ,$$
(1.2)

and for $\lambda = 3$

$$\exp[h_{n+1}(S_1 \cdot S_2)]$$
$$= \exp(-g_n) \int\int dS_3 \, dS_4 \exp[3^{d-1}(h_n(S_1 \cdot S_3) + h_n(S_3 \cdot S_4) + h_n(S_4 \cdot S_2))]$$
(1.3)

with

$$\exp g_n = \int dS \exp[2^d h_n(S_1 \cdot S)] \qquad \text{(for } \lambda = 2) ,$$
(1.4)

$$h_{n+1}(1) = h_n(1) = 0 .$$
(1.5)

For numerical work it is easier to use the coefficients obtained by expanding in Legendre polynomials:

$$\exp[-\lambda^{d-1}V(\varphi)] = \sum_{l=0}^{\infty} (2l+1)\mu_l P_l(\cos \varphi) ,$$
(1.6)

$$V(\varphi) \equiv -h(\cos \varphi) .$$
(1.7)

The equation $h_{n+1}(1) = h_n(1) = 0$ or equivalently $V(0) = 0$ gives the normalisation

$$\sum_{l=0}^{\infty} (2l+1)\mu_l = 1 .$$
(1.8)

The Migdal transformation for the Legendre coefficients can now be written as the consequetive application of R_d and R_b ($d-1$ times), followed by the multiplication with a normalisation factor:

$$\mu' = (D(\mu))^{-\lambda^{d-1}} R_b^{d-1} R_d(\mu) ,$$
(1.9)

where R_d is given by

$$\tilde{\mu} = R_d(\mu) \quad \text{with} \quad \tilde{\mu}_m = \mu_m^{\lambda}$$
(1.10)

and R_b by

$$\bar{\mu} = R_b(\mu)$$

with for $\lambda = 2$

$$\bar{\mu}_m = \sum_{l_1 = 0}^{\infty} \sum_{l_2 = 0}^{\infty} (2l_1 + 1)(2l_2 + 1)\begin{pmatrix} m & l_1 & l_2 \\ 0 & 0 & 0 \end{pmatrix}^2 \mu_{l_1} \mu_{l_2} \tag{1.11}$$

and for $\lambda = 3$

$$\bar{\mu}_m = \sum_{l_1 = 0}^{\infty} \sum_{l_2 = 0}^{\infty} \sum_{l_3 = 0}^{\infty} \sum_{l_4 = 0}^{\infty} (2l_1 + 1)(2l_2 + 1)(2l_3 + 1)(2l_4 + 1)$$

$$\times \begin{pmatrix} l_4 & l_1 & l_2 \\ 0 & 0 & 0 \end{pmatrix}^2 \begin{pmatrix} m & l_4 & l_3 \\ 0 & 0 & 0 \end{pmatrix}^2 \mu_{l_1} \mu_{l_2} \mu_{l_3} . \tag{1.12}$$

The normalisation factor is expressed in terms of

$$D(\mu) = \sum_{l=0}^{\infty} (2l + 1)\mu_l^{\lambda} \tag{1.13}$$

$\begin{pmatrix} m & l_1 & l_2 \\ 0 & 0 & 0 \end{pmatrix}$ is a Wigner $3 - j$ symbol [5].

All numerical work was done on mapping (1.9) with $\lambda = 2, 3$ and $d = 2, 3$. The cut-offs used were 20 up to 50 (all μ_m with m greater than the cut-off were set equal to zero). The results were insensitive to the value of the cut-off, except for the coordinates (not the spectrum) of the low-temperature fixed points.

In the next section we shall discuss the low-temperature phases and the possible phase transitions between them. The two-dimensional model is treated in section 3 and the three-dimensional one in section 4. In both cases all phase transitions are studied and the flow diagram is sketched. In section 5 we derive the magnetic exponents for both the Heisenberg and XY-model in three dimensions. A discussion of the results and our conclusions are presented in section 5.

2. Low-temperature behaviour

For the d-dimensional XY model we could show [3] that at low temperature the Gaussian line was a flow line of the Migdal transformation. We will show here that the same is true for the Heisenberg model. The Gaussian line, parametrized by b, is defined, slightly different from the XY-case, by

$$\mu_l = b \, e^{b/4} \, e^{-b(l + \frac{1}{2})^2} . \tag{2.1}$$

Again it is trivial to show that the transformation R_d (eq. (1.10) with $\lambda = 2$) maps a point $b = b_0$ on this line into $b' = 2b_0$. For small b_0 a point $b = b_0$ is mapped into $b = \frac{1}{2}b_0$ by R_b (eq. (1.11)). To prove this we need again a continuum approximation as used in ref. [2] and some additional approximations.

The Wigner coefficient occurring in eq. (1.11) is defined by [5]

$$
\begin{pmatrix} m & l_1 & l_2 \\ 0 & 0 & 0 \end{pmatrix}^2 = \frac{(S-2m)!(s-2l_1)!(S-2l_2)!}{(S+1)!}
$$
$$
\times \left[\frac{(\frac{1}{2}S)!}{(\frac{1}{2}S-m)!(\frac{1}{2}S-l_1)!(\frac{1}{2}S-l_2)!} \right]^2 , \tag{2.2}
$$

$$
S \equiv m + l_1 + l_2 , \tag{2.3}
$$

where S has to be even and m, l_1, l_2 should satisfy the triangle conditions

$$
S - 2m \geqslant 0 , \qquad S - 2l_1 \geqslant 0 , \qquad S - 2l_2 \geqslant 0 . \tag{2.4}
$$

If the quantities in eq. (2.4) are not only positive but also much greater than one, we can use Stirling's formula to approximate the right-hand expression in eq. (2.2), giving

$$
\begin{pmatrix} m & l_1 & l_2 \\ 0 & 0 & 0 \end{pmatrix}^2 \approx \frac{2}{\pi} \left[S(S-2m)(S-2l_1)(S-2l_2) \right]^{-1/2} . \tag{2.5}
$$

We now replace the discrete variables $2m + 1$, $2l_1 + 1$, $2l_2 + 1$ by resp. x, u, v, from which we find, writing $t = \frac{1}{2}(x + u + v)$:

$$
\begin{pmatrix} m & l_1 & l_2 \\ 0 & 0 & 0 \end{pmatrix}^2 \approx \frac{1}{2\pi} \left[t(t-x)(t-u)(t-v) \right]^{-1/2} \equiv \frac{1}{2\pi} \Delta^{-1}(x, u, v) . \tag{2.6}
$$

Writing $\mu_{l_1} = z(u)$, etc. eq. (1.11) becomes

$$
\bar{z}(x) = c \int_0^\infty \int_0^\infty du\, dv\, uv\Delta^{-1}(x, u, v)z(u)z(v) , \tag{2.7}
$$

where for the moment the value of the constant c is irrelevant. Notice that $\Delta(x, u, v)$ is just the area of a triangle with sides x, u, v (it is possible to form a triangle with these sides because of the conditions (2.4)).

We now perform a coordinate transformation from u^2, v^2 to w, y defined by (see also fig. 1)

$$
u^2 = w^2 + (y - \tfrac{1}{2}x)^2 ,
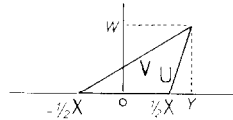$$
$$
v^2 = w^2 + (y + \tfrac{1}{2}x)^2 , \tag{2.8}
$$

Fig. 1. The coordinate transformation (2.8): $u^2 = w^2 + (y - \frac{1}{2}x)^2$, $v^2 = w^2 + (y + \frac{1}{2}x)^2$ with Jacobian $-8\Delta(x, u, v)$ which is minus eight times the area of the triangle with sides x, u and v.

with Jacobian $-4xw = -8\Delta(x, u, v)$. Eq. (2.7) becomes, apart from a constant factor,

$$\bar{z}(x) = \int\limits_{-\infty}^{+\infty} dy \int\limits_{0}^{\infty} dw \, z(\sqrt{w^2 + (y - \tfrac{1}{2}x)^2}) z(\sqrt{w^2 + (y + \tfrac{1}{2}x)^2}) . \tag{2.9}$$

From this equation it is easy to see that $z(x) \sim e^{-bx^2}$ is mapped into $\bar{z}(x) \sim e^{-\frac{1}{2}bx^2}$. Discretising $e^{-\frac{1}{4}bx^2}$ gives $e^{-b(l+\frac{1}{2})^2}$, which is the form postulated in eq. (2.1). The factor $b \, e^{+b/4}$ follows from the normalisation condition (eq. (1.8)).

Analogously to the XY case [2] a scale invariant fixed point can be found in the continuum approximation but this will not be studied here.

We will now investigate what kind of low-temperature phases and associated phase transitions are possible. In the XY model [2, 3] there were infinitely many Gaussian fixed points (or lines, for $d = 2$) lying on stable Gaussian flow lines given by

$$\mu_{nl} = \mu_0 \, e^{-b(nl)^2} , \qquad n \text{ fixed integer}, \quad \text{all other } \mu_m \text{ zero}. \tag{2.10}$$

For Heisenberg spins this is only true for $n = 1$ and $n = 2$. No other periodicity will be preserved because of the presence of the Wigner coefficient in eq. (1.11) instead of a Kronecker-delta as in the case of XY spins [2, 3, 7]. A starting point of the form (2.10), i.e. μ_l is only different from zero if l is an n-fold, will not retain its form because some $\bar{\mu}_m$ for which m is not an n-fold (for instance $\bar{\mu}_2$) will become non-zero and the original period n will be lost already after one renormalisation-step. The case $n = 2$ is special because the sum of the three numbers occurring in the Wigner 3-j symbol has to be even which means that the μ_l with even and odd l will mix in a special way.

If we start with μ_l of the form (α is a normalisation constant)

$$\mu_{2l} = \alpha \, e^{-b(2l - \frac{1}{2})^2} ,$$
$$\mu_{2l+1} = a\alpha \, e^{-b(2l + \frac{3}{2})^2} , \tag{2.11}$$

this form will be preserved by eqs. (1.11) and (1.12), at least for small b. The

mapping for a is the same one as for the XY case and can be translated [3] to the Migdal transformation for the coupling constant of the Ising model. The only possible phase transitions are therefore ferromagnetic and antiferromagnetic Ising transitions (the antiferromagnetic ones only with odd scale factor.) As an example, take $d = 2$ and scale factor $\lambda = 3$ for which the equation for a reads

$$a' = \frac{3a^3 + a^9}{1 + 3a^6} . \tag{2.12}$$

In the limit $b \to 0$ the cases $a > 1$ and $a < -1$ correspond to imaginary potentials so we restrict ourselves to $-1 \le a \le 1$. The stable fixed points of this interval $[-1, 1]$ are $a = 1$ (ferromagnetic phase), $a = 0$ (nematic or disordered Ising phase), $a = -1$ (antiferromagnetic phase). For a picture of the spin configurations of these phases see fig. 1 in ref. [3]. Ising phase transitions take place at $a = \pm(-\frac{1}{2} + \frac{1}{2}\sqrt{5})$. The existence of all these fixed points of the eq. (2.11) was verified numerically.

If we take a period n other than two for the μ_l:

$$\mu_{nl+i} = a_i \alpha \, e^{-b(nl+i+\frac{1}{2})^2} \tag{2.13}$$

with n a fixed integer greater than two and $i = 0, 1, \ldots, n - 1$, then this period will not be preserved under the mapping (1.9). Numerically we checked for $\lambda = 2$ and $d = 3$ that for any starting point of the form (2.13) with small b, the mapping will bring this point to one of the low-temperature fixed points of the form (2.11) with $b \to 0$ and a either zero or plus one (the only stable fixed points for an even scale factor) or to the high-temperature fixed point. In particular no antinematic phase [4] can be found in the Migdal approximation, even with an odd scale factor. We searched numerically for a possible non-Gaussian antinematic fixed point but we did not succeed. We will further discuss this problem in sections 3 and 4.

In the next two sections the special cases $d = 2$ and $d = 3$ will be studied in the whole temperature region.

3. Two-dimensional Heisenberg model

A Gaussian point as defined in eq. (2.1) is mapped onto itself for $d = 2$ in the continuum approximation (b is doubled by R_d and halved by R_b so fixed under $R_b R_d$, see eq. (1.9)). As in the XY case [2] the spectrum of the Gaussian line can be calculated exactly in the continuum approximation. To compute the

eigenvalues we omit the normalisation factor $D(\mu)$ in the mapping (1.9) (with $\lambda = 2$, $d = 2$) which gives an extra eigenvalue four which should be discarded afterwards (this method is justified in ref. [2] for XY spins; the case studied here is completely analogous). The Jacobi matrix M_{ll_1} becomes (we now write z_l instead of μ_l to distinguish between the normalised and not normalised mapping)

$$M_{ll_1} = 4 \sum_{l_2=0}^{\infty} (2l_1 + 1)(2l_2 + 1)\begin{pmatrix} l & l_1 & l_2 \\ 0 & 0 & 0 \end{pmatrix}^2 z_{l_1} z_{l_2}^2 , \tag{3.1}$$

which gives z_{l_1} as an eigenvector with eigenvalue 4. In the continuum approximation we find

$$M(x, y) = \frac{4y}{\pi} \int_{|x-y|}^{x+y} \frac{u \, du}{\Delta(x, y, u)} \, z(y) z^2(u) . \tag{3.2}$$

Substituting $z(x) = z_0 \, e^{-bx^2}$ gives

$$M(x, y) = \frac{16by}{\pi} \, e^{-by^2} \int_{|x-y|}^{x+y} \frac{e^{-2bu^2}}{\Delta(x, y, u)} \, u \, du . \tag{3.3}$$

Using $\Delta(x, y, u) = \frac{1}{4}[((x + y)^2 - u^2)(u^2 - (x - y)^2)]^{1/2}$ and eq. 3.364 from ref. [6] we derive

$$M(x, y) = 32by \, e^{-b(2x^2+3y^2)} I_0(4bxy) . \tag{3.4}$$

The solution of the eigenvalue problem

$$\int_0^{\infty} M(x, y)v_n(y)dy = \lambda_n v_n(x) \tag{3.5}$$

can now be found using eq. 7.421.4 from ref. [6] ($I_0(x) = J_0(ix)$) giving

$$\left.\begin{aligned} v_n(x) &= e^{-bx^2} L_n(3bx^2) \\ \lambda_n &= 4 \cdot \left(\tfrac{1}{4}\right)^n \end{aligned}\right\} \quad n = 0, 1, 2, \ldots \tag{3.6}$$

The spectrum is the same as that for the Gaussian line in the two-dimensional XY model [2]. The eigenvalue four has to be omitted (because mapping (1.9) is normalised) so the largest eigenvalue is one. The Gaussian line is therefore a stable fixed line in the continuum approximation. This, however, does not settle the problem for the discrete mapping. For the

two-dimensional XY model the Gaussian line was an almost fixed line [2] of the discrete mapping. The corrections, due to the discreteness of the mapping, which we measured by $\chi^2 \equiv \Sigma_l (\mu_l' - \mu_l)^2$, were exponentially small [2, 7]:

$$\chi^2 = \sqrt{\frac{8\pi}{b}} \, \exp(-\pi^2/2b) \, . \tag{3.7}$$

Note that in ref. [2] the prefactor in this formula was incorrect. The deviation in fig. 1 in ref. [2] due to the change in the prefactor is negligible. Although the Gaussian line was exactly fixed only in the limit $b \to 0$, the form of χ^2 as given in eq. (3.7) was interpreted [2, 7] as an indication of the presence of a Kosterlitz–Thouless phase transition [8]. No such transition is expected for the two-dimensional Heisenberg model [8]. There is indeed much evidence [9] that no phase transition occurs at finite temperature for the pure Heisenberg model defined by

$$\mathcal{H} = K \sum_{(i,j)_{\text{n.n.}}} (S_i \cdot S_j) \, . \tag{3.8}$$

Recently some authors [10] have found indications for a finite-temperature phase transition in the two-dimensional Lebwohl–Lasher model,

$$\mathcal{H} = K \sum_{(i,j)_{\text{n.n}}} (S_i \cdot S_j)^2 \tag{3.9}$$

but others [11] found a negative result. The model (3.8) was studied in the Migdal approximation by Migdal [1] himself and Ogilvie [12]. The latter defined an effective temperature T and found for the change of T under the renormalisation mapping at low temperatures:

$$\frac{\mathrm{d}T}{\mathrm{d}l} \sim T^2 \, . \tag{3.10}$$

This effective temperature T should correspond to our b (eq. (2.1)) at low temperatures. We studied numerically the model (2.11) using the mapping (1.9) with scale factor $\lambda = 2$. With the models (3.8) and (3.9) as starting points repeated application of the mapping caused these points to approach the Gaussian flow lines of the form (2.11) with $a = 1$ and $a = 0$ respectively. As expected the Gaussian lines were not exactly fixed lines and eventually every point was mapped towards the high-temperature fixed point $\mu_l = \delta_{l,0}$. We calculated χ^2 (defined above eq. (3.7)) along these lines numerically and found for both $a = 0$ and $a = 1$ (see fig. 2)

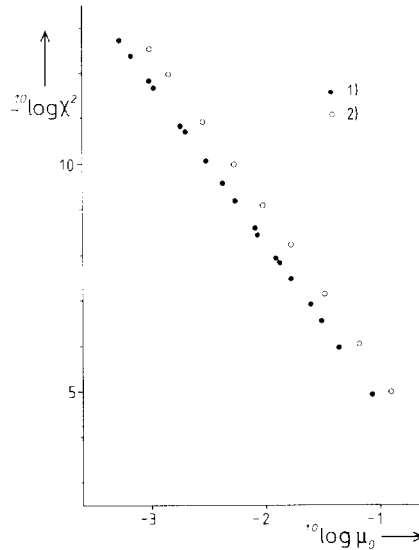$$\chi^2 \sim b^{7/2} \, , \tag{3.11}$$

Fig. 2. Plot of $\log \chi^2 = \log(\Sigma_i(\mu'_i - \mu_i)^2)$ against $\log \mu_0$ ($\approx \log b$ at low temperatures) for the two-dimensional Heisenberg model with the potential corresponding to eq. (2.11) with 1) $a = 1$ and 2) $a = 0$.

which is essentially the same result as eq. (3.10), analytically derived in ref. [12] for model (3.8). This correction is growing much faster for increasing b than the XY result, eq. (3.7). We expect therefore that no phase transition is present at finite temperature for both models (3.8) and (3.9). Because no other Gaussian low-temperature fixed points exist than the ones occurring in model (2.11), as shown in section 2, we can conclude that no finite-temperature phase transition exists for any two-dimensional Heisenberg model, independent of the form of the potential. We also studied model (3.9) with the sign of K such that the potential has a minimum for $\varphi = \pm \frac{1}{2}\pi$. We find that for all temperatures the model is mapped towards the high-temperature phase. Not even a zero-temperature fixed point exists for this model.

The complete flow diagram for general two-dimensional Heisenberg models is shown in fig. 3. It is only a small part of the one for XY models presented by us in ref. [3].

4. Three-dimensional Heisenberg model

In three dimensions the flow along the Gaussian lines is directed to low temperatures (the mapping is now $R_b R_b R_d$ so b is halved with each step, see section 2). The low-temperature fixed point structure, which was unstable
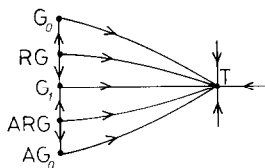
Fig. 3. Complete flow diagram for two-dimensional Heisenberg models with general isotropic interaction. T is the high-temperature fixed point ($\mu_l = \delta_{l,0}$), G_0 and AG_0 the ferro- and antiferromagnetic ordered Ising points, RG and ARG govern the ferro- and antiferromagnetic low-temperature Ising transition and G_1 denotes the disordered Ising point (nematic order for the continuous spins). For a picture of the spin configurations of some of these phases see fig. 1 in ref. [3].

towards higher temperature for $d = 2$ (fig. 3), is therefore stable for $d = 3$ (in fact for any $d > 2$). Just as in the XY case [3] we have therefore intermediate-temperature fixed points, governing the phase transitions which exist between the low- and high-temperature phases. Some parts of the flow diagram were found earlier [4, 13, 14], but here the complete diagram will be presented.

We performed a numerical search for the unstable intermediate-temperature fixed points by minimizing χ^2. The eigenvalues of a fixed point were obtained by diagonalizing the Jacobi-matrix in the point. The existence of only two respectively three stable low-temperature fixed points was reestablished (for scale factor $\lambda = 2$ respectively 3), as well as the flow along the Gaussian lines and the Ising low-temperature phase transition. We found for $\lambda = 2$ three intermediate-temperature fixed points: P_1 [4, 13] governing the transition between the ferromagnetic ordered Ising phase and the paramagnetic phase, P_2 [4, 14] governing the transition between the disordered Ising or nematic phase and the paramagnetic phase (for a picture of the spin arrangement in the different phases see fig. 1 in ref. [3]) and the new point P_* with two relevant eigenvalues. For odd scale factor P_1 and P_2 get antiferromagnetic twinpoints AP_1, AP_* (for every solution μ_l also $(-1)^l \mu_l$ is a solution for odd scale factor). The complete flow diagram is shown in fig. 4. Only the essential flow lines (separatrices, stable and unstable manifolds) have been drawn. The whole
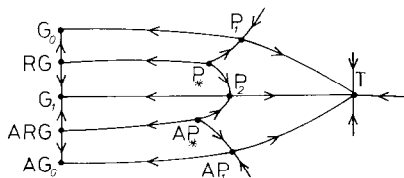

Fig. 4. Complete flow diagram for three- (and presumably higher-) dimensional Heisenberg models with general isotropic interaction. The low temperature fixed points are described in the subscript of fig. 3 and in section 2. For the intermediate-temperature fixed points see tables I–IV.

phase space is infinite dimensional but we assume that the part shown here attracts all other orbits. Analytical calculations (section 2) and numerical searching suggest strongly that indeed no other fixed points exist. We expect a similar flow diagram for any $d > 2$.

The largest eigenvalues λ_i of the fixed points for scale factor $\lambda = 2$ are given in table I. The results for the low-temperature points are not very precise, because there the effect of the cutoff will always be felt, as was discussed in ref. [3].

The Legendre coefficients μ_l of the intermediate-temperature fixed points are given in table II, and the Fourier coefficients ν_l of the corresponding potentials in table III.

If we denote the potential corresponding to P_1 by $V_1(\varphi)$ we can also write the potentials $V_2(\varphi)$ and $V_*(\varphi)$ corresponding to P_2 and P_* in terms of $V_1(n\varphi)$:

Table I
The three largest eigenvalues of all fixed
points of mapping (1.9) for $d = 3$, $\lambda = 2$.

	λ_1	λ_2	λ_3
G_0	0.15	$1.6\,E - 3$	$7\,E - 4$
G_i	0.15	$1.6\,E - 3$	$7\,E - 4$
RG	1.92	0.15	$4.4\,E - 2$
P_1	1.8119	0.2638	$2.344\,E - 2$
P_2	1.9866	0.2758	$2.317\,E - 2$
P_*	2.1518	1.6471	0.3739
T	0	0	0

Table II
The Legendre coefficients of the intermediate-temperature
fixed points, defined by

$$\exp(-4V(\varphi)) = \sum_{l=0}^{\infty} (2l + 1)\mu_l P_l(\cos \varphi) .$$

	P_1	P_2	P_*
μ_0	0.50027	0.39926	0.29576
μ_1	0.13141	0	$0.58603\,E - 1$
μ_2	$0.18614\,E - 1$	$0.94315\,E - 1$	$0.66902\,E - 1$
μ_3	$0.16438\,E - 2$	0	$0.12644\,E - 1$
μ_4	$0.97367\,E - 4$	$0.12693\,E - 1$	$0.86359\,E - 2$
μ_5	$0.40500\,E - 5$	0	$0.14775\,E - 2$
μ_6	$0.12234\,E - 6$	$0.10659\,E - 2$	$0.69626\,E - 3$
μ_7	$0.27554\,E - 8$	0	$0.10763\,E - 3$
μ_8	$0.47243\,E - 10$	$0.59831\,E - 4$	$0.37579\,E - 4$
μ_9	$0.627\quad E - 12$	0	$0.52523\,E - 4$
μ_{10}	$0.65\quad E - 14$	$0.23476\,E - 5$	$0.14205\,E - 5$

Table III

The Fourier coefficients of the potentials corresponding to
the intermediate-temperature fixed points, defined by

$$V(\varphi) = \sum_{l=-\infty}^{\infty} \nu_l \cos l\varphi \; .$$

	P_1	P_2	P_*
ν_0	0.20298	0.19452	0.28068
ν_1	−0.10418	0	−0.53007 E − 1
ν_2	0.28096 E − 2	−0.99774 E − 1	−0.90456 E − 1
ν_3	−0.12808 E − 3	0	0.10993 E − 2
ν_4	0.68573 E − 5	0.26233 E − 2	0.21644 E − 2
ν_5	−0.39539 E − 6	0	−0.60111 E − 4
ν_6	0.23803 E − 7	−0.11594 E − 3	−0.86630 E − 4
ν_7	−0.14747 E − 8	0	0.37039 E − 5
ν_8	0.9329 E − 10	0.60100 E − 5	0.40507 E − 5
ν_9	−0.600 E − 11	0	−0.23358 E − 6
ν_{10}	0.41 E − 12	−0.33537 E − 6	−0.20318 E − 6

$$V_2(\varphi) \approx 0.95771 V_1(2\varphi) + 0.00065 V_1(4\varphi) + 0.00006 V_1(6\varphi) + \cdots , \tag{4.1}$$

$$V_*(\varphi) \approx 0.50881 V_1(\varphi) + 0.88199 V_1(2\varphi) - 0.01118 V_1(3\varphi) + 0.0034 V_1(4\varphi) . \tag{4.2}$$

A plot of $V_1(\varphi)$ is shown in fig. 5.

We have numerically constructed the phase diagram for the two-parameter potential (in fact a linear combination of (3.8) and (3.9)):

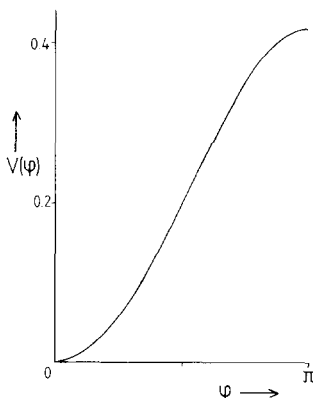$$V_1(\varphi) = -K_1 \cos \varphi - K_2 \cos 2\varphi . \tag{4.3}$$

Fig. 5. Plot of $V_1(\varphi)$, the potential corresponding to P_1 (see tables II, III).

It is shown in fig. 6. This phase diagram can be explained using the flow diagram of fig. 4: the low-temperature transition between the ferromagnetic (ordered Ising, G_0) and nematic phase (disordered Ising, G_1) is a three-dimensional Ising transition (governed by RG); the transitions from the ferromagnetic and nematic phase to the high temperature phase (T) are governed by P_1 and P_2 while the tricritical point is governed by P_*. For discretised three-dimensional spins this model was studied with Migdal renormalisation in ref. [15], giving comparable results for dense enough discretisation.

The critical exponents ν, defined by $\nu = \log 2 / \log \lambda_{max}$ for scale factor two, for the transitions associated with P_1 and P_2 are given by

$$P_1: \quad \nu = 1.166 , \tag{4.4}$$

$$P_2: \quad \nu = 1.010 . \tag{4.5}$$

As expected, these results are not in agreement with the "exact" results: $\nu = 0.705$ [16] for the ferromagnetic transition (compare with (4.4)). Also the transition from the nematic to the disordered phase should be first order [17, 18] whereas a second order transition is found here with ν given in (4.5).

The critical coupling for the pure $\cos \varphi$ model ($K_2 = 0$ in (4.3)) is in this Migdal approximation given by
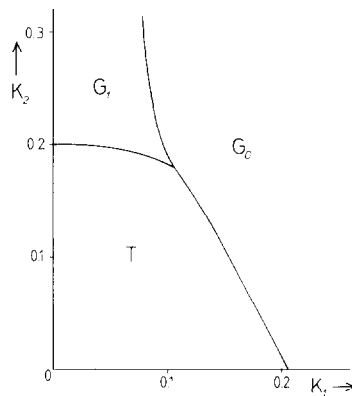
$$K_1 = 0.205 , \tag{4.6}$$

Fig. 6. Phase diagram for the potential $V(\varphi) = -K_1 \cos \varphi - K_2 \cos 2\varphi$ for Heisenberg spins on a three-dimensional lattice. The phases are denoted by T (disordered high temperature phase), G_0 (ferromagnetic order) and G_1 (nematic order), see also fig. 1 in ref. [3].

and for the pure $\cos 2\varphi$ model ($K_1 = 0$ in (4.3))

$$K_2 = 0.200 . \tag{4.7}$$

The "exact" results for the simple cubic lattice (Migdal renormalisation gives the same results for different lattice types) are $K_1 = 0.6925$ [19] and $K_2 = 0.668$ [18]. (Note that $P_2(\cos \varphi) = \frac{3}{4} \cos 2\varphi + \frac{1}{4}$ if a comparison is made with ref. [18].) The couplings (4.6) and (4.7) found with Migdal are roughly a factor 3.4 smaller than the exact values, which is the same factor [3] as found for the three-dimensional Ising and XY model (see also table VII in section 6).

Our Migdal results (4.4) and (4.6) for the pure $\cos \varphi$ model are in agreement with those of ref. [13] (the critical coupling differs a factor two because there the mapping $R_b R_d R_b$ was used instead of $R_b R_d R_d$, see ref. [3]). Our results for the $\cos 2\varphi$ model (or Lebwohl–Lasher model), (4.5) and (4.7), differ somewhat from the results in ref. [14] because these authors did not use [14] the full Migdal equations. Our results here extend those of a previous study by us [4]: a new fixed point P_* is found and the complete flow diagram is constructed.

Again we also studied the antinematic potential $V(\varphi) = + K \cos 2\varphi$. We normalised to $V(\frac{1}{2}\pi) = 0$ in this case. This potential is mapped to the high-temperature one for all values of K, even for $K = \infty$ (zero temperature). We did not find any stable or unstable fixed point in the neighbourhood of $K \cos 2\varphi$, indicating again the absence of an antinematic phase in the Migdal approximation.

5. Magnetic exponents

In this section we compute the magnetic exponents of the intermediate-temperature fixed points of both the three-dimensional Heisenberg model, as discussed in section 4, and the three-dimensional XY model, treated before in ref. [3].

Consider the following Hamiltonian:

$$\beta \mathcal{H} = \sum_{(i,j)_{n.n.}} V(S_i \cdot S_j) + m \sum_i \cos \theta_i , \tag{5.1}$$

with $m \ll 1$ the strength of the magnetic field and θ_i the angle between S_i and the direction of the magnetic field. Migdal renormalisation is ambiguous [20] in treating site-terms like magnetic or ordering field. We choose to follow Migdal [1] and moved the site terms along with the bonds. If we now perform Migdal renormalisation on (5.1) we have to generalise the form of the potential: V no

longer depends only on $(S_i \cdot S_j)$, but becomes a more general function of $S_i \cdot S_j$ which is still symmetric. $(V(S_i, S_j) = V(S_j, S_i))$.) After one renormalisation step the Hamiltonian is of the form

$$\beta \mathcal{H} = \sum_{(i,j)_{\text{n.n.}}} V'(S_i, S_j) + \lambda^y m \sum_i \cos \theta_i + \mathcal{O}(m^2) \tag{5.2}$$

with λ the scale factor and y the magnetic exponent. For any fixed point the magnetic exponent can now be derived [13, 14] as (here for $\lambda = 2$)

$$2^y = 2^{d-1}\left(1 + \frac{\bar{\mu}_1}{\bar{\mu}_0}\right) \tag{5.3}$$

with $\bar{\mu} = R_b(\mu)$ for both the XY and the Heisenberg model. For the Heisenberg model μ_l is the fixed point of mapping (1.9) with $\lambda = 2$ (R_b defined by eq. (1.11)) and corresponds to the potential $V(\varphi)$ according to eq. (1.6). For the XY model μ_l is the fixed point of eq. (1.8) in ref. [3] (R_b defined by eq. (1.10) in ref. [3]) and corresponds to the potential $V(\varphi)$ according to eq. (1.5) in ref. [3].

The magnetic exponents can be generalised by considering an ordering field of the form $m \cos n\theta$ (again $m \ll 1$, n an integer) instead of $m \cos \theta$. We can derive the analog of eq. (5.3) (see also refs. [13, 14]):

$$2^{y_n} = 2^{d-1}\left(1 + \frac{\bar{\mu}_n}{\bar{\mu}_0}\right). \tag{5.4}$$

We have listed the first four exponents for the intermediate-temperature fixed points of the three-dimensional Heisenberg model in table IV and for the XY-model in table V.

The agreement with the "exact" results for y_1 is quite good, which is also the case for the two- and three-dimensional Potts model (table 1, in ref. [21]), as shown in table VI.

Table IV
Magnetic exponents of the intermediate-temperature fixed points of the 3D Heisenberg model, P_1, P_2, P_* (see tables I–III).

	y_1	y_2	y_3	y_4
P_1	2.5514	2.1811	2.0378	2.0056
P_2	2.0	2.5470	2.0	2.1764
P_*	2.5486	2.5482	2.2442	2.1766

Table V
Magnetic exponents of three of the intermediate-temperature fixed points of the 3D XY model (see tables II, III in ref. [3]).

	y_1	y_2	y_3	y_4
V_1	2.5559	2.1524	2.0237	2.0025
V_2	2.0	2.5559	2.0	2.1524
$A_{1,2}$	2.5544	2.5550	2.2272	2.1506

Table VI
Comparison of the Migdal approximation with exact results for the first magnetic exponent for different models. The exact results are from ref. [16]. For the Migdal Ising exponents see for instance ref. [21], for the XY and Heisenberg results see tables IV and V and also ref. [13].

Model	Exact y_1	Migdal ($\lambda = 2$)y_1
2D Ising	1.8750	1.8791
3D Ising	2.4843	2.5650
3D $XY(V_1)$	2.4833	2.5559
3D Heis(P_1)	2.4830	2.5514

Our results for V_1 and P_1 (table VI) are in agreement with those of ref. [13], obtained with the same method. y_2 of P_2 (table IV) differs from the value of ref. [14], because there the Migdal renormalisation with some further approximations is used. The Migdal result for this last exponent (y_2 of P_2) is spurious anyway, because the phase transition is first order for this model [14, 17, 18] with $y_2 = 3$.

6. Discussion and conclusions

We used Migdal renormalization to analyse general Heisenberg spin models like we did earlier for XY spins [2, 3]. We found again that the Gaussian line was a flow line of the mapping and that all low temperature fixed points were Gaussian.

At low temperatures only Ising transitions are possible as opposed to the XY case where all $Z(N)$ transitions exist [3]. The low temperature fixed points are unstable towards higher temperature for $d < 2$ and stable for $d > 2$. Also for $d = 2$ these points are unstable and the flow on the Gaussian lines away from these points is much faster than in the XY case [7, 2] (see section 3), indicating that no Kosterlitz-Thouless transition takes place for the two-dimensional pure Heisenberg model ($V(\varphi) \sim \cos \varphi$) or Lebwohl–Lasher model ($V(\varphi) \sim \cos 2\varphi$).

For $d = 3$ the intermediate-temperature fixed points, governing the phase transitions between high- and low-temperature phases, were calculated numerically. The complete flow diagram was constructed and was found to be in agreement with earlier results in refs. [4, 13, 14]. The phase diagram for a potential of the form $K_1 \cos \varphi + K_2 \cos 2\varphi$ was also constructed. In the literature we could not find a Monte Carlo or mean field phase diagram to compare

Table VII

The quotient of the exact critical coupling and the Migdal one with scale factor $\lambda = 2$ for various three-dimensional models on a simple cubic lattice. The Migdal results can be found in ref. [21] (Potts model), ref. [3] (XY model) and eqs. (4.6) and (4.7) in this paper. The exact results are from refs. [22] (1- and 4-state Potts), [23] (Ising), [24] (3-state Potts), [25] (XY), [19] (Heis, $\cos \varphi$) and [18] (Heis, $\cos 2\varphi$). The numbers between parentheses denote the estimated error in the last decimal.

Model	$K_{exact}/K_{Migdal, \lambda = 2}$
1-state Potts	3.43(3)
2-state Potts (Ising)	3.40
3-state Potts	3.34
4-state Potts	3.32(6)
$XY(K \cos \varphi)$	3.41(2)
Heis($K \cos \varphi$)	3.38(1)
Heis($K \cos 2\varphi$)	3.34(1)

with, as was done for a similar phase diagram for XY spins [3]. We found surprisingly good agreement with Monte Carlo results in that case after rescaling the Migdal diagram. In table VII it is shown that the quotients of the exact critical coupling (obtained from Monte Carlo simulations or series analysis) and the Migdal critical coupling (for scale factor $\lambda = 2$) do not vary by more than a few percent for various three-dimensional models (both with discrete and continuous spins).

In spite of the fact that this constancy is not understood, but encouraged by the success for planar spins, we would therefore suggest that fairly accurate phase diagrams can be obtained, also for Heisenberg spins, by using Migdal renormalisation and rescaling with a factor 3.37. However, for the model $V(\varphi) = + K \cos 2\varphi$ (with minima at $\varphi = \pm \frac{1}{2}\pi$) Migdal renormalisation predicts no phase transition (section 4), not even at zero temperature, while Kohring and Shrock [26] found a second order transition at finite temperature using Monte Carlo simulations. At this moment we do not understand why the Migdal approximation gives reliable quantitative results for some models but is unable to give a phase transition in other cases. It seems worth investigating if Migdal renormalisation also fails to predict a phase transition for other models with nonzero disordering ground state energy [26].

In cases where reliable phase diagrams are obtained the temperature exponents are not reliable, as usual, and first order transitions will be seen as second order ones. The magnetic exponents (for both Heisenberg and XY

spins), corresponding to second order phase transitions, are in good agreement with exact results.

References

[1] A.A. Migdal, Sov. Phys. JETP 42 (1976) 743.
[2] K. Sokalski, Th.W. Ruijgrok and B. Schoenmaker, Physica A 144 (1987) 322.
[3] B. Schoenmaker, Physica A 151 (1988) 124.
[4] K. Sokalski and Th.W. Ruijgrok, Physica A 130 (1985) 412.
[5] See for instance: M. Rotenberg, R. Bivins, N. Metropolis and J.K. Wooton, The 3-j and 6-j symbols (The Technology Press, Mass. Inst. of Techn., 1959).
[6] I.S. Gradsteyn and I.M. Ryzhik, Table of Integrals, Series and Products (Academic Press, New York, 1965).
[7] J.V. José, L.P. Kadanoff, S. Kirkpatrick and D.R. Nelson, Phys. Rev. B 16 (1977) 1217.
[8] J.M. Kosterlitz and D.J. Thouless, J. Phys. C 6 (1973) 1181.
[9] A.A. Belavin and A.M. Polyakov, JETP Lett. 22 (1975) 245.
E. Brezin and J. Zinn-Justin, Phys. Rev. Lett. 36 (1976) 691.
S.H. Shenker and J. Tobochnik, Phys. Rev. B 22 (1980) 4462.
[10] S. Solomon, Phys. Lett. B 100 (1981) 492.
M. Fugukita et al., Phys. Lett. B 109 (1982) 209.
C. Chiccoli, P. Pasini and Z. Zannoni, Physica A 148 (1988) 298.
[11] S. Sinclair, Nucl. Phys. B205 (1982) 173.
[12] M.C. Ogilvie, Nucl. Phys. B190 (1981) 791.
[13] C. Jayaprakash, G.A. Jongeward and P. Shukla, Phys. Rev. B 18 (1978) 5112.
[14] P. Shukla and T.J. Sluckin, J. Phys. A 18 (1985) 93.
[15] A. Margaritis, G. Odor and A. Patkös, J. Phys. A 20 (1987) 1917.
[16] J.C. Le Guillou and J. Zinn-Justin, Phys. Rev. Lett. 39 (1977) 95.
[17] P.A. Lebwohl and G. Lasher, Phys. Rev. A 6 (1972) 426.
[18] U. Fabbri and Z. Zannoni, Mol. Phys. 58 (1986) 763.
[19] S. McKenzie, C. Domb and D.L. Hunter, J. Phys. A 15 (1982) 3899.
[20] T.W. Burkhardt, in: Real Space Renormalisation, T.W. Burckhardt, J.M.J. van Leeuwen, eds. (Springer, Berlin, 1982).
[21] H.H. Chen, Felix Lee and H.C. Tseng, Phys. Rev. B 34 (1986) 6448.
[22] F.Y. Wu, Rev. Mod. Phys. 54 (1982) 235.
[23] M.N. Barber et al., Phys. Rev. B 32 (1985) 1720.
[24] W.G. Wilson and C.A. Vause, Phys. Rev. B 36 (1987) 587.
[25] M. Ferer, M.A. Moore and M. Wortis, Phys. Rev. B 8 (1973) 5205.
[26] G. Kohring and R.W. Shrock, Nucl. Phys. B295 (1988) 36.